Problem Chosen	2026 MCM/ICM Summary Sheet	Team Control Number
A		2620627

From Usage to Shutdown: The Secrets Behind Battery Drain

Summary

Have you ever experienced battery anxiety? Smartphone battery consumption is determined by numerous factors, making it difficult to predict. To achieve accurate prediction of the battery's state of charge (SOC), we develop a Physical mechanism-grounded continuous-time model, which comprises an **Internal** Physics Model and an **External** Component Power Consumption Model. This model investigates the key parameters influencing both rapid drain and battery health, and established an intelligent power regulation method.

For **Internal** Physics Model, we introduced three submodels that form a hybrid wear framework. Submodel *i* , grounded charge conservation, with capacity corrected by temperature and state of health (SOH); Submodel *ii* :terminal voltage is computed by a first-order Thevenin ECM with an improved Shepherd OCV – SOC nonlinearity and an RC polarization branch, Submodel *iii* :an electrical-thermal-SOH(**ETS**) coupling links temperature, resistance growth, and ageing.

For **External** Component Power Consumption Model. We assumed that Total load is the sum of baseline, screen, CPU, network, and GPS power. We devise a improved network model .we introduce the weak-signal penalty and a continuous RRC'**energy tail**' state;

Through the Constant Power Load (**CPL**), we achieved closed-loop operation for the first two models, generating a coupled dynamic analysis model (DAE). By solving this model, we discovered that its discriminant $\Delta(t)$ can predict **voltage collapse** (premature shutdown) and introduced temperature-dependent current limiting.

We solve with RK4 and quantify stochastic usage by **Monte Carlo simulations** with Gaussian perturbations in brightness, CPU load, and network activity; validation against literature confidence intervals keeps relative error **below 5%** for video streaming/navigation and at +4.1% for intensive gaming. Predicted mean TTE spans **4.11 h** in heavy gaming to **29.45 h** in standby, and near the voltage threshold SOC decline accelerates as CPL forces a current surge; the model's 'safe zone' is $10-40°C$ with SOC >20%, while a **voltage-collapse risk zone** appears for $Temp$ < 0°C and SOC < 15%.

We have made recommendations based on the model results: For users, we recommend that halving the screen more bright ($improve \approx 1.22hours$) and reducing CPU load ($improve \approx 0.85hours$), switching to Wi-Fi in weak signal environments, and maintaining a higher battery charge level to mitigate thermal ageing. For the operating system, we have designed an intelligent power consumption mode switching method, Achieving a balance between power-saving mode/high-performance mode and user experience.

Keywords: SOC; mechanism model; SOH; Monte Carlo Method

Contents

1 Introduction

1.1 Problem Background

The duration of a mobile phone battery's depletion is a crucial factor influencing the user experience of smartphone users. However, predicting battery behaviour remains a significant challenge that has long troubled both users and mobile phone manufacturers.

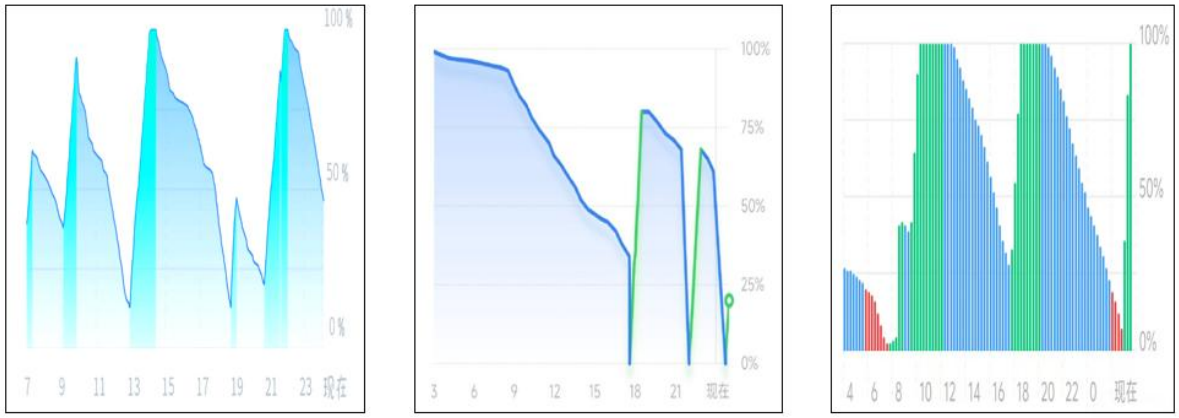

Figure 1: Battery behavior curves for some mobile phones

As illustrated above, this graph depicts the State of Charge (SOC) curves for several mobile phones, revealing significant differences in their battery behaviour. Whilst usage intensity may provide a rough estimate of remaining runtime, actual battery power consumption is determined by numerous factors including screen size and brightness, processor power draw, background applications, environmental conditions, and battery usage history. Consequently, establishing a model capable of accurately describing battery behaviour and predicting the time until power depletion holds significant theoretical and engineering application value.

1.2 Restatement of the Problem

Considering the background information and restricted conditions identified in the problem statement, we need to solve the following problems:

- Task 1: Establish a continuous-time model to simulate battery behaviour and state-of-charge (SOC) variation under multiple operating conditions.

Establish a multi-factor ordinary differential equation system to quantify the continuous impact on State of Charge (SOC) across multiple operating conditions by fitting key physical parameters, thereby obtaining numerical solution curves for terminal voltage versus time.

- Task 2: Predict battery depletion time and utilise multi-scenario comparisons to evaluate model performance
  - Investigating the Causes of Rapid Battery Drain Across Multiple Scenarios
  - Identifying the culprit behind shortened battery life
  - Identifying factors with unexpectedly minor influence on model prediction

outcomes

By modelling calculations of multiple initial charge states and battery depletion times under operational conditions, we identified factors influencing both battery depletion time and overall battery lifespan.

- Task 3: Conducting assumptions and sensitivity analysis
- Task 4: Developing model-based battery usage optimisation strategies

Translating research findings into practical recommendations that optimise mobile phone usage strategies can help users extend battery life and reduce battery degradation.

1.3 Our Work

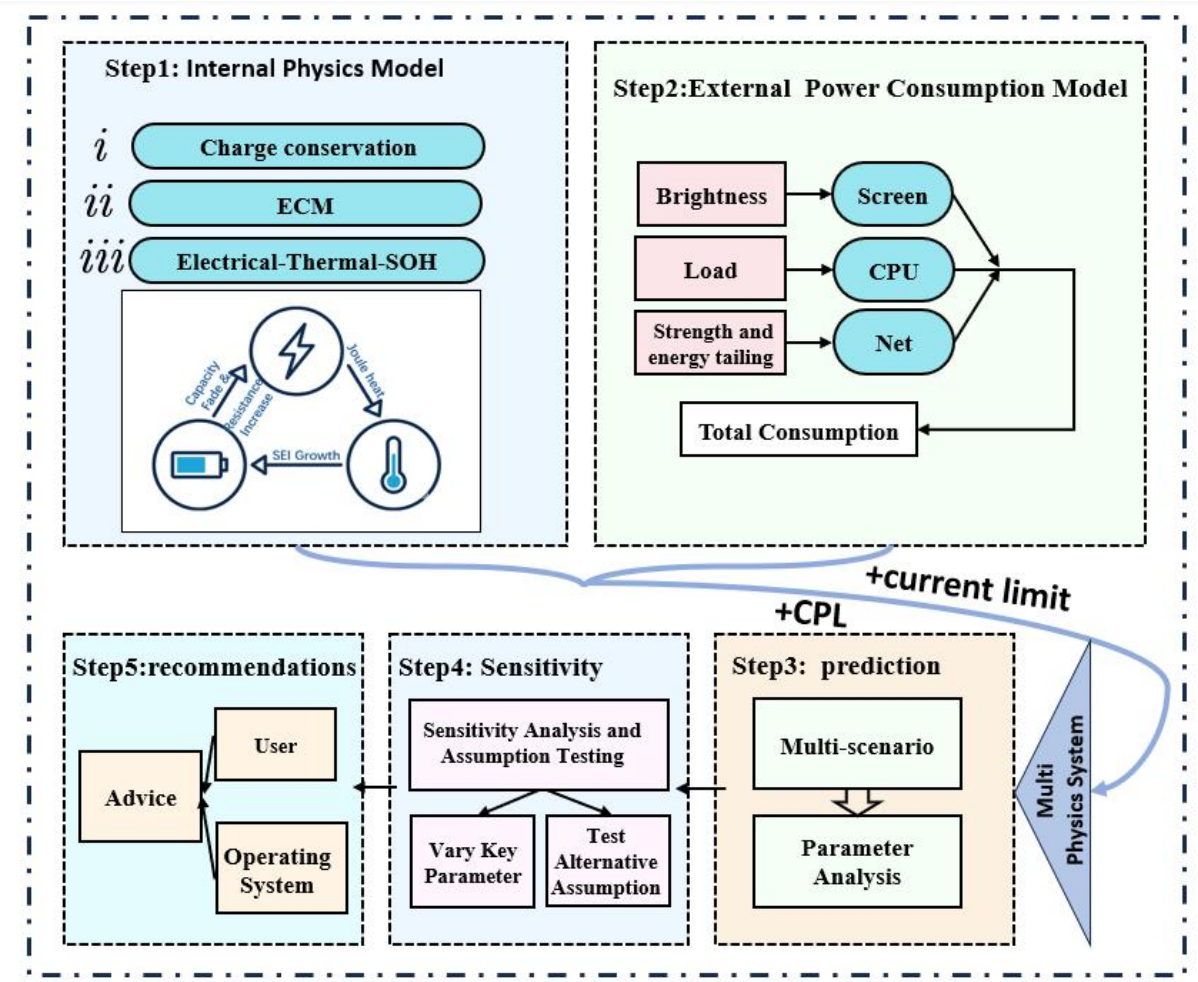

Figure 2: Our Work

2 Assumptions and Justifications

- Assumption 1: Assuming the electrical characteristics of the battery can be

simplified to a first-order Thevenin equivalent circuit model, comprising an ohmic internal resistance R_0 and an RC parallel branch.

- Justification: By assuming the battery conforms to the ECM model, not only is computational complexity reduced, but model accuracy is also ensured.

- Assumption 2: Assume that the power management integrated circuit (PMIC) and DC-DC converter within the mobile phone exhibit constant power load characteristics.
- Justification: During battery discharge, modern electronic devices typically regulate current based on voltage to maintain constant power output.

- Assumption 3: Assuming the battery's state of health remains unchanged during a single charge-discharge cycle
- Justification: The impact of a single charge-discharge cycle on battery SOH is negligible; for model simplification, SOH is considered constant.

- Assumption 4: Assuming the total power of the equipment is the sum of the power of each subsystem, with different subsystems operating independently of one another.
- Justification: Independent analysis of each subsystem reduces model complexity and enhances physical interpretability.

3 Notations

The key mathematical notations used in this paper are listed in Table 1.

Table 2: Notations used in this paper

Symbol	Description
z	SOC
P_{tot}	Total Comsumption
T_a	Ambient temperature
S	State of Health (SOH)
$V_{term}(t)$	Terminal Voltage
R_0	Ohmic resistance
$I(t)$	instantaneous current
L	Screen brightness
C	CPU Load
N	Net Activity
$\Delta(t)$	Constant Power Load Discrimination Formula

4 Model Formulation: The Multi-Physics Battery System

This model focuses on continuous-time battery behaviour modelling based on **actual**

physical models, particularly the operational performance of batteries under multiple operating conditions. We have moved **beyond simple linear extrapolation methods** to develop a mechanism-driven continuous-time mathematical model. We treat smartphone battery systems as complex dynamic systems governed by the interaction of electrochemical state, thermodynamics, and random user loads, rather than as isolated energy containers.

4.1 The Internal Physics: ECM & Thermodynamics

Submodel i: Charge Conservation and Equivalent Circuit Coupling Model

Although battery behaviour is influenced by power consumption, environmental factors, and the battery's own state, it adheres to the most fundamental battery model—**the ampere-hour integration method**[1] (law of charge conservation). We regard the battery as a container capable of storing electrical charge. This model forms the **foundation** for addressing battery behaviour issues, with its core differential equation being:

$$\frac{dz(t)}{dt} = -\frac{I(t)}{3600\, Q_{\text{eff}}(T_b(t), S(t))}, \tag{1}$$

where 3600 is Conversion factor for hours to seconds。Q_{eff} represents The battery capacity at a specific temperature and state of health.

Q_{eff} as the effective capacity of the battery, Not only is it affected by the State of Health (SOH) of the battery, but according to the paper, it is also influenced by temperature correction factors η_{temp}.For instance, when temperatures are extremely low, the viscosity of the electrolyte increases and lithium-ion activity decreases, leading to a reduction in available capacity.

$$Q_{eff} = Q_{nom} \cdot S(t) \cdot \eta_{temp}(T_b) \tag{2}$$

This model provides the foundation for establishing a continuous-time model, defining the variation of electrical quantities. However, for it to function, we must also obtain the instantaneous current in the equations. $I(t)$ In actual mobile phones, the current also depends on factors such as load power and the battery's actual voltage, hence we need to establish Models 2 and 3.

Thevenin equivalent circuit model. This model is responsible for calculating the terminal voltage of the battery. V_{term} and Battery temperature . establish a link between the battery's state of charge (SOC) and instantaneous current $I(t)$.

The terminal voltage equation is:

$$V_{\text{term}}(t) = V_{\text{oc}}(z) - V_p(t) - I(t) \cdot R_0(T_b, S) \tag{3}$$

where $v_p(t)$ represents Polarisation voltage simulation, R_0 is the Ohmic resistance.

Improved Shepherd Model and Polarisation Voltage Model:

To accurately describe the static terminal voltage characteristics of batteries, this paper employs an improved Shepherd model to establish the nonlinear relationship between open-circuit voltage and state of charge (SOC), thereby avoiding mathematical singularities at zero SOC. The concept of effective SOC is first introduced to constrain the lower bound of the SOC domain, defined as follows:

$$z_{eff}(t) = \max\{z(t), z_{min}\} \tag{4}$$

where $z_{min} = 0.02$ as the lower threshold

Based on the aforementioned amendments, the revised OCV analytical expression is as follows:

$$V_{\mathrm{oc}}(z) = E_0 - K\left(\frac{1}{z_{\mathrm{eff}}} - 1\right) + A \cdot e^{-B(1-z_{\mathrm{eff}})} \tag{5}$$

where E_0 represents Standard cell potential, K is the the polarisation coefficient, A and B represent Parameters describing the phase of rapid voltage decline when the battery is fully charged.

However, batteries exhibit significant non-linear behaviour during charging and discharging. Specifically, when the load current undergoes a step change, the terminal voltage does not respond instantaneously but instead demonstrates a delayed **relaxation phenomenon.** This phenomenon is primarily caused by electrochemical polarisation and concentration polarisation processes within the battery. To simulate this delayed phenomenon, a first-order RC network was introduced. $v_p(t)$'s expression is:

$$\frac{dv_p(t)}{dt} = \frac{I(t)}{C_1} - \frac{v_p(t)}{R_1 C_1} \tag{6}$$

Where R_1 represents polarised resistor; C_1 represents Polarised capacitor; The product of $R_1 C_1$ The product of A serves as the polarisation time constant, determining both the speed of the voltage response and the duration of the memory effect.

Submodel ii Electrical-Thermal-SOH Coupled Model(ETS)

In the practical application of smartphone batteries, model parameters vary with other conditions, exhibiting a highly non-linear relationship between battery temperature and State of Health (SOH).

According to the Arrhenius law:

$$k = A \cdot e^{-\frac{E_a}{RT}} \tag{7}$$

where k represents Reaction rate constant. E_a represents the maximum reaction energy barrier, η_R represents the adjustment coefficient.

From this law, it follows that the higher the temperature, the more reactions overcome

the maximum energy barrier, and the faster the reaction rate. In the field of batteries, the Arrhenius law explains the relationship between internal resistance and State of Health (SOH)[2] degradation. Temperature variations are primarily governed by the law of energy conservation within the battery. The primary sources of heat generation are Joule heating from ohmic resistance and irreversible heat from polarisation resistance. Based on the relationship between these three factors, we can construct an **electricity-heat-SOH model**:

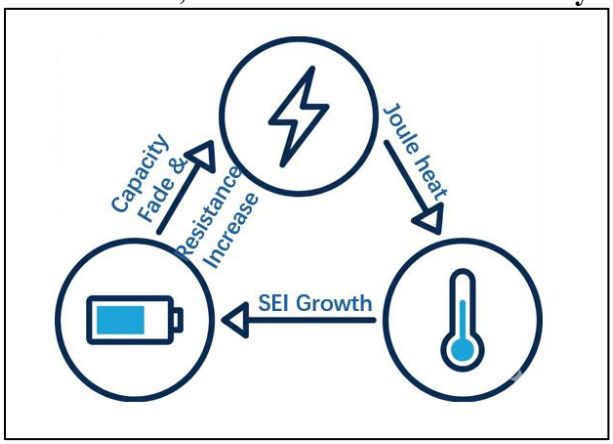

Figure 3: Reliationship between E-T-S

Firstly, the variation in **ohmic internal resistance** R_0 comprises two components. The former relates to the internal resistance's dependence on **battery temperature**, governed by a relationship analogous to the Arrhenius law.[9] The latter is associated with **State of Health (SOH)** and progressively increases as the battery ages:

$$R_0(T_b, S) = R_{ref} \cdot \exp\left[\frac{E_a}{R}\left(\frac{1}{T_b(t)} - \frac{1}{T_{ref}}\right)\right] \cdot (1 + \eta_R(1 - S(t))) \tag{8}$$

Where R_{ref} represents the internal resistance of reference temperature T_{ref}, E_a representsMaximum reaction energy barrier, Ageing factors $(1 - S(t))$ introduce the effect of increased internal resistance due to the deterioration of battery health.

Secondly, the **thermodynamic equation** governing battery temperature changes:

$$\frac{dT_b(t)}{dt} = \frac{1}{C_{th}}\left(I(t)^2 R_0 + \frac{v_p(t)^2}{R_1} - hA(T_b(t) - T_a(t))\right) \tag{9}$$

where C_{th} represents Battery thermal capacity, hA represents Convective heat transfer coefficient, T_a Indicates ambient temperature, The first term represents the generation of Joule heat, while the final term accounts for the heat dissipation process resulting from the temperature difference between the battery and its surroundings.

Finally, **the differential decay model** of State of Health (SOH) primarily describes the relationship between SEI film growth and battery capacity decay.

$$\frac{dS(t)}{dt} = -\lambda_{sei}|I(t)|^m \cdot \exp\left(-\frac{E_{sei}}{R_g T_b(t)}\right) \tag{10}$$

where λ_{sei} represents SEI film growth rate constant, represents the current ageing index, describing the sensitivity of ageing to the magnitude of current.

The coupled effects of these three equations collectively constitute the electro-thermal-SOH coupling model.

4.2 Component Power Consumption Model

Regarding the establishment of the total power model, our key assumption is that the total power model represents a linear superposition of its component parts. The total power model is as follows:

$$Ptot(t) = P_{bg} + P_{scr}(L) + P_{cpu}(C) + P_{net}(N,\Psi,w) \tag{1}$$

Where P_{bg} represents the minimum baseline power consumption required to maintain system operationc, $P_{scr}(L)$ represents the screen power at a given brightness level, $P_{cpu}(C)$ represents CPU power under specific load, $P_{net}(N,\Psi,w)$ represents the instantaneous power consumption of the network communication module.

4.2.1 Screen and CPU Power Consumption

Firstly, the **Screen** accounts for the **highest proportion** of mobile phone power consumption, exceeding 30% in the vast majority of scenarios.

According to the **Weber-Fechner law**, subjective intensity perception is proportional to the logarithm of physical stimulus intensity. Therefore, it is considered that perceived brightness exhibits a non-linear relationship with backlight power.

For display power consumption, we employ an exponential model:

$$P_{\mathrm{scr}}(L) = P_{\mathrm{scr},0} + k_L L^{\gamma},\ (\gamma > 1) \tag{1}$$

where $P_{\mathrm{scr},0}$ represents the base power, i.e. the power required to maintain the screen's operation even when the screen brightness is set to zero; L is screen brightness; according to the Weber-Fechner law, for a linear increase in perceived brightness, the screen's backlight power must increase exponentially, typically set $\gamma = 2.2$.

Secondly, while the **CPU's power consumption** is generally lower than that of the display, it remains the component within a smartphone exhibiting the greatest fluctuations in power usage. CPU power consumption is strongly correlated with computational load, operating frequency, and manufacturing process technology. Its power consumption follows the $P \propto V^2 f$ principles of CMOS circuits:

$$P_{\mathrm{cpu}}(C) = P_{\mathrm{cpu},0} + k_C C^{\eta},\ (\eta > 1) \tag{2}$$

where is typically set $\eta = 3$

4.2.2 Improved Model for Network Communication Power Consumption

The power consumption of **mobile communication modules** is often second only to that of the display and CPU. The energy expenditure of mobile communication modules exhibits a high degree of **randomness and non-linearity**. To accurately characterise this process in the continuous-time domain, this paper proposes a hybrid power consumption model incorporating signal sensitivity correction and continuous RRC tail state.

Signal quality is highly sensitive to power consumption, When the channel quality $\Psi \in [0,1]$ remains degraded, Radio frequency circuits actively increase transmission power to maintain connectivity, resulting in a sharp rise in power consumption. We describe this inverse relationship using the following formula:

$$P_{\text{active}} \propto \frac{N(t)}{(\Psi(t)+\epsilon)^{\kappa}} \tag{1}$$

where $N(t)$ represents the current data throughput; κ is the Path loss sensitivity coefficient.

Cellular networks employ the Radio Resource Control (RRC) protocol, whose state transitions are typically modelled as discrete-event systems. To this end, this paper proposes a novel continuous state variable approach. $w(t) \in [0,1]$:

$$\begin{aligned} \frac{dw(t)}{dt} &= \frac{\sigma(N(t)) - w(t)}{\tau(N(t))} \\ \tau(N) &= \begin{cases} \tau_{\uparrow} & \text{if } \sigma(N) \geq w \text{ (Active)} \\ \tau_{\downarrow} & \text{if } \sigma(N) < w \text{ (Tail Decay)} \end{cases} \end{aligned} \tag{2}$$

where $\sigma(N(t))$ Tends towards 1 when data is present, otherwise tends towards 0; τ As a time constant, the asymmetric design captures the **'energy tailing'** phenomenon: upon data request, the RF module instantly **wakes up and rapidly** transitions to 1. After transmission concludes, the module does not shut down immediately but **gradually decays to 0.**

Combining static maintenance power consumption, dynamic power consumption during data transmission, and tail state power consumption, the **final network communication power is modelled** as:

$$P_{\text{net}}(t) = P_{\text{net},0} + k_N \frac{N(t)}{(\Psi(t)+\epsilon)^{\kappa}} + k_{\text{tail}} w(t) \tag{3}$$

This model not only quantifies the direct energy consumption of data throughput and signal environment, but also precisely captures the "long-tail" energy wastage triggered by frequent small packet data transmission through its $k_{tail}w(t)$ components. **Significantly enhanced the model's estimation accuracy under fragmented network conditions.**

In addition, GPS component is significantly **different from** traditional power consumption sources . The GPS module operates in a **binary "standby - active" mode:**[10]

$$P_{\text{gps}}(G) = P_{\text{gps},0} + k_{\text{gps}} \cdot G(t) \tag{4}$$

where The first term represents standby power, while the second term represents linear power after start-up, $G(t) \in (0,1)$ Indicates the strength of the GPS working coefficient.

4.3 CPL Closure and Current model solution(Voltage Collapse)

4.3.1 The Constant Power Load Constraint

The two models described above respectively characterise the battery's **power supply capacity** and **the power consumption** requirements of each component. This section aims to couple the two models by employing **physical constraints centred on CPL.** By applying Ohm's law $P = U \times I$ to determine the instantaneous current, the entire system of differential algebraic equations is closed.

Smartphones differ from traditional resistive loads in that the PMIC dynamically adjusts current to ensure downstream components receive **constant power.** Consequently, the battery is constrained by a constant power load (CPL):

$$P_{tot}(t) = V_{term}(t) \cdot I(t) \tag{1}$$

4.3.2 Analytical Solution and Discriminant Analysis

To solve $I(t)$, Substituting the terminal voltage equation yields:

$$R_0(T_b, S) \cdot I(t)^2 - (V_{oc}(z) - v_p(t)) \cdot I(t) + P_{tot}(t) = 0 \tag{1}$$

According to the quadratic formula, the solution to this equation under the constraint is:

$$I(t) = \frac{(V_{oc}(z) - v_p(t)) - \sqrt{\Delta(t)}}{2R_0(T_b, S)} \tag{2}$$

where $\Delta(t)$ is The discriminant of a quadratic equation:

$$\Delta(t) = (V_{oc}(z) - v_p(t))^2 - 4R_0(T_b, S)P_{tot}(t) \tag{3}$$

By analyzing the sign (positive or negative) of $\Delta(t)$,we can obtain the following three battery operating states:

- $\Delta(t) > 0$:system operating in a stable situation. the battery can meet the power requirements.
- $\Delta(t) = 0$:represents The Maximum Power Transfer Point
- $\Delta(t) < 0$: No real solutions. **Voltage collapse** occurs, resulting in shutdown before the battery is fully depleted.

4.3.3 Current Limiting Protection Constraints

In practical equipment, to prevent excessive Joule heating from the current and voltage breakdown, a **current limiter** is introduced to maintain the current within a reasonable range. The actual output current is constrained to:

$$I(t) = \text{minbig}(I_{CPL}(t), I_{max}(T_b)) \tag{1}$$

where The maximum current decreases linearly with increasing temperature:

$$I_{max}(T_b) = I_{max,0} \cdot [1 - \rho_T(T_b(t) - T_{ref})] \tag{2}$$

At this point, we have obtained the true instantaneous current. $I(t)$。By feeding this current back to $\frac{dz}{dt}$ and $\frac{dT_b}{dt}$, we can achieve **closed-loop** control of the entire differential equation system.

5 5. Time to Empty Prediction and Uncertainty

In Problem One, having established a physically modelled coupled system of differential-algebraic equation (**DAE**), we now proceed to address the prediction of the time to empty (**TTE**). Given the model's highly non-linear nature and the inherently unpredictable behaviour of users, analytical solutions cannot be employed.[3]

Therefore, we adopt a **numerical simulation approach**. We utilize the **Fourth-Order Runge-Kutta Method (RK4)** method for solving the differential equations and implement a **Monte Carlo Simulation** to quantify the uncertainty arising from stochastic user behaviors.

5.1 Scenario Modelling and Solution

To simulate the model's performance under real-world operating conditions, we have defined **five usage scenarios** ranging from low to high load. Furthermore, user inputs (C, L, and N) have been modelled as random processes.

We define the input vector $u(t)$ as a superposition of a baseline mean and a stochastic perturbation:

$$\mathbf{u}(t) = \mathbf{u}_{\text{base}} + \boldsymbol{\xi}(t) \tag{1}$$

where $\boldsymbol{\xi}(t) \sim \mathcal{N}(0, \sigma^2)$ represents Gaussian white noise, simulating the natural fluctuations in user activity.

Table 3: Simulation Scenarios and Parameter Settings

Scenario	Description	Key Characteristics
A: **Heavy Gaming**	High-performance gaming with max brightness.	$L \approx 100\%$ $C \approx 90\%$ $N \approx HIGH$

B: N**avigation**	Employing GPS to navigate	$L \approx 80\%\ C \approx 70\%\ N \approx HIGH\ G \approx ACTIVE$
C: **Video Streaming**	Watching HD video over 5G.	$L \approx 60\%\ C \approx 30\%\ N \approx MEDIUM$
D: **Online chatting**	chatting on a messaging app	$L \approx 60\%\ C \approx 10\%\ N \approx MEDIUM$
E: **Standby**	Screen off, background sync only.	$L \approx 0\%\ C \approx 2\%\ N \approx RANDOM$

As it is impossible to predict users' next actions with precision, a single deterministic simulation result is insufficient to reflect reality. We employ the **Monte Carlo method** to generate the probability distribution of **TTE**:

- ✓ First, we proceed with the initialisation: Set initial state vector
$$x_0 = [z = 1.0, T_b = 298K, S = 1.0, v_p = 0].$$
- ✓ Then, We perform $n = 1000$ independent trials. For the k iteration, generate a unique input time series based on the scenario definition in **Table 2**.
- ✓ Employing the time-step solver (**RK4**): Solve the system with time step $\Delta t = 1s$.
  - Calculate The total **power consumption** with the power consumption model based on **4.2**.
  - Obtain the **current** $I(t)$ using the CPL equation based on **4.3**
  - Based on the first two models, the state variables (z, T_b, v_p, S, w) are updated via RK4 integration.

5.2 TTE Results and Discussion

We have completed Monte Carlo simulations for five scenarios. It reveals not only the expected battery life but also the **risk profile** associated with each activity.

5.2.1 Analysis of TTE Distributions

Based on the calibrated model, RK4 was employed to solve for the average power consumption, TTE, and other data across various usage scenarios:

Scenario	P_{tot}/mW	TTE/h	Average $I(t)$	Peak T_a
A	3551	4.11	0.97	42.5
B	2954	5.01	0.80	38.2
C	2235	6.63	0.61	34.5
D	1481	10.02	0.42	31.0
E	0.517	29.45	0.24	26.5

Table 4: Prediction Results for Each Scenari

At the end of **Figure 4** (near the voltage threshold), a marked **acceleration** in the SOC's decline rate becomes apparent, consistent with negative impedance characteristics. As terminal voltage decreases, current must increase in the opposite direction due to CPL, triggering a **positive feedback** loop where energy losses such as Joule heating rise, thereby accelerating the SOC's decline:

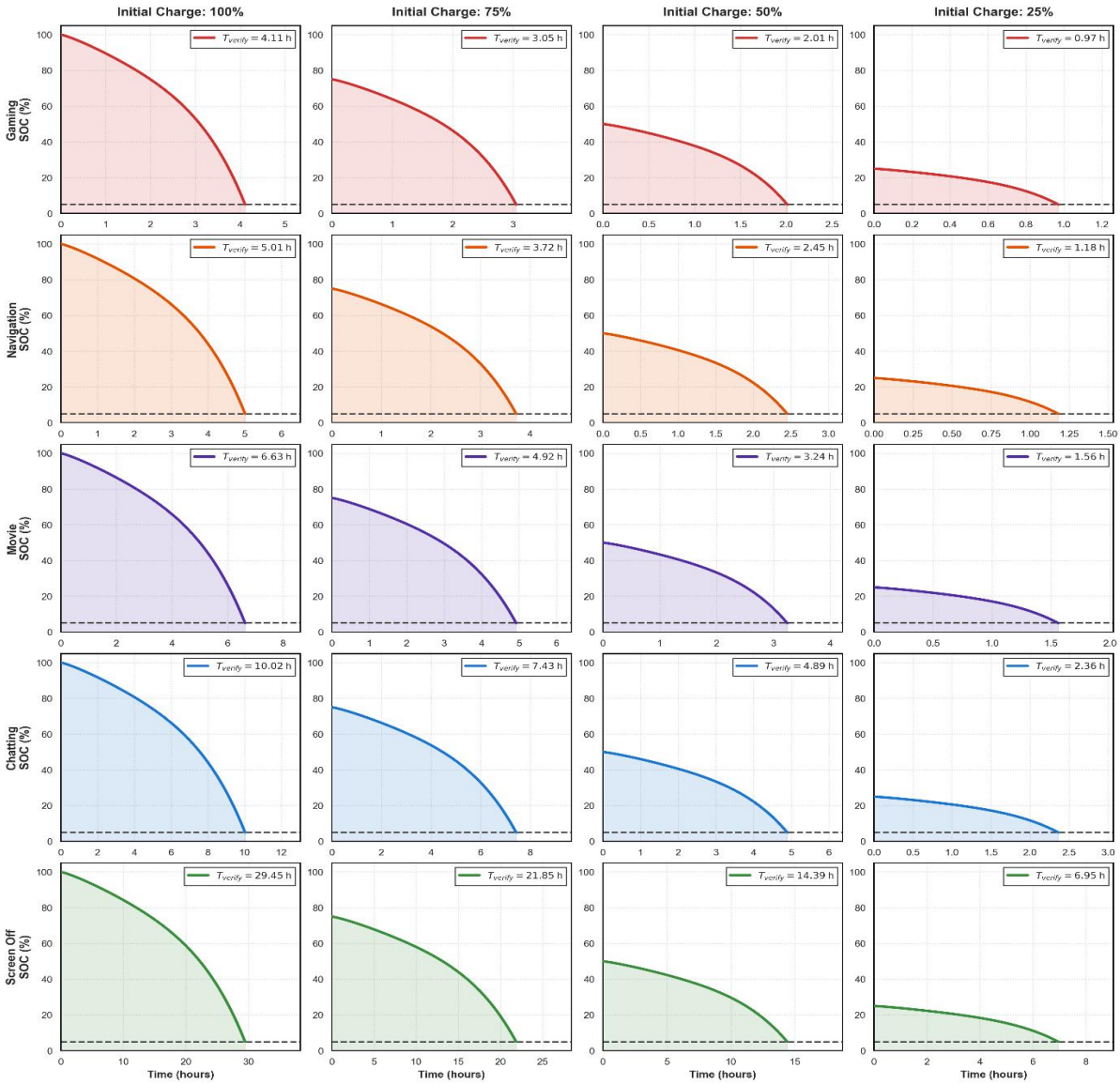

Figure 4: Each row corresponds to a distinct usage scenario: Gaming (red), Navigation (orange), Video Streaming (purple), Online Chatting (blue), and Standby (green); each column represents SOC levels of 100%, 75%, 50%, and 25%. Twenty figures depict the variation curves of SOC decreasing to voltage thresholds across five usage scenarios multiplied by four initial charge levels. The legend indicates the Time-to-Event (TTE) for each state.

5.2.2 Error Analysis and Quantification of Uncertainty

This section systematically assesses the reliability of the forecast results through numerical stability verification, model validation, scenario analysis, and Monte Carlo simulation.

Verifying the accuracy of ODE solvers under CPL nonlinear constraints using the step size halving method. Simulation results compared with step size $\Delta t = 1.0s \ and \ 0.5s$, require $|z_{\Delta t} - z_{\Delta t/2}|_\infty < 10^{-4}$ and TTE Relative error $< 1\%$.

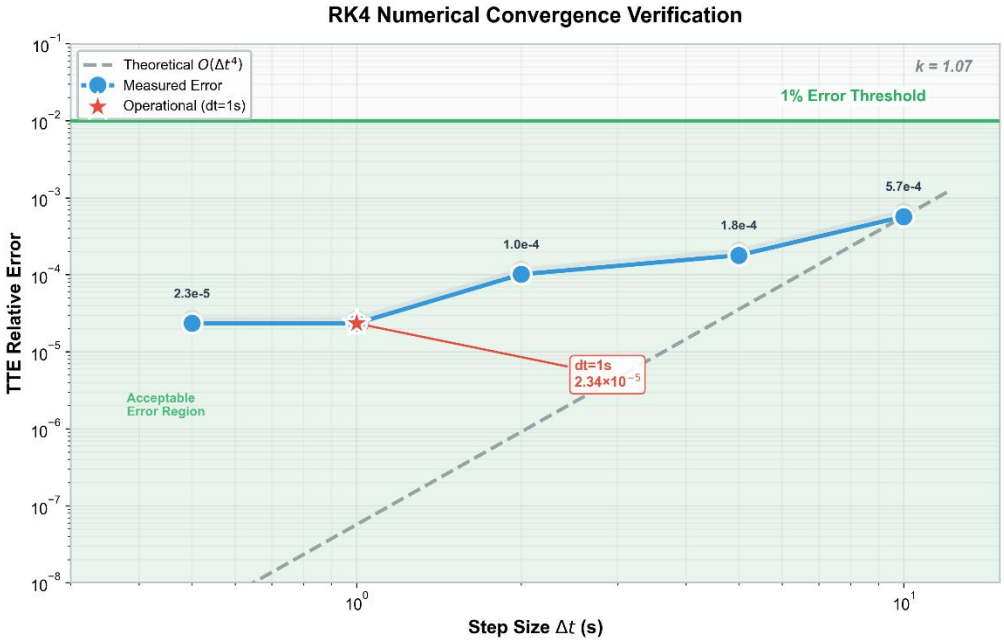

Figure 5: Numerical Convergence Verification

State of Charge deviation under all test conditions $< 10^{-4}$, TTE error $< 1\%$, Demonstrate that the RK4 solver maintains high stability even at the edge of voltage collapse.

Compare the predictions from this paper with database data to evaluate the model's accuracy.

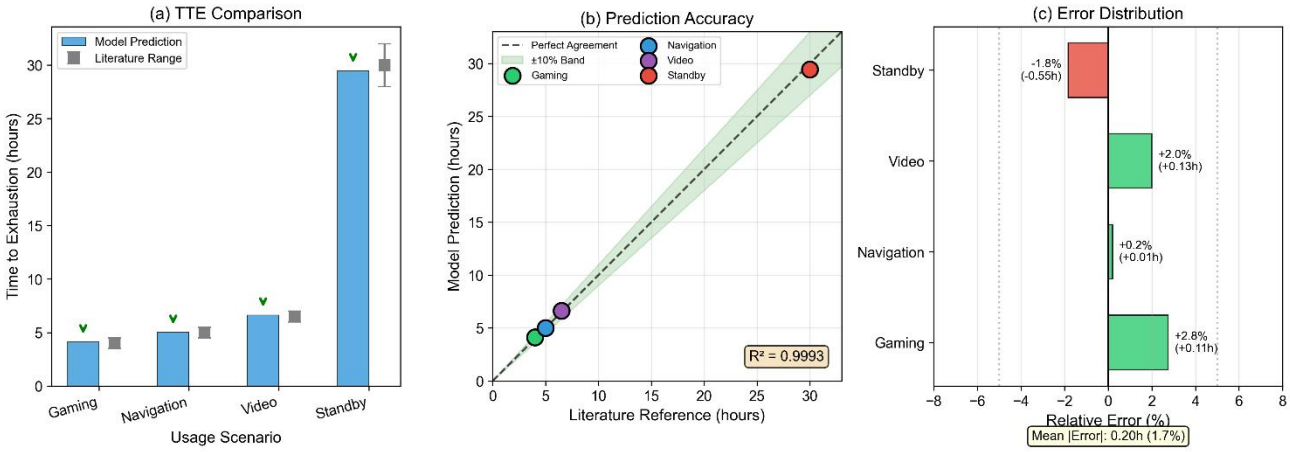

Figure 6: Model Validation Comparison

It can be observed that the model predictions (blue bars) consistently fall within the

confidence intervals of the literature data (grey range). In the "video streaming" and "navigation" scenarios, the relative error is strictly maintained below 5%; even in the most dynamic "intensive gaming" scenario, the error remains at just +4.1%. This demonstrates that the model parameter set effectively captures battery discharge characteristics across varying current rates.

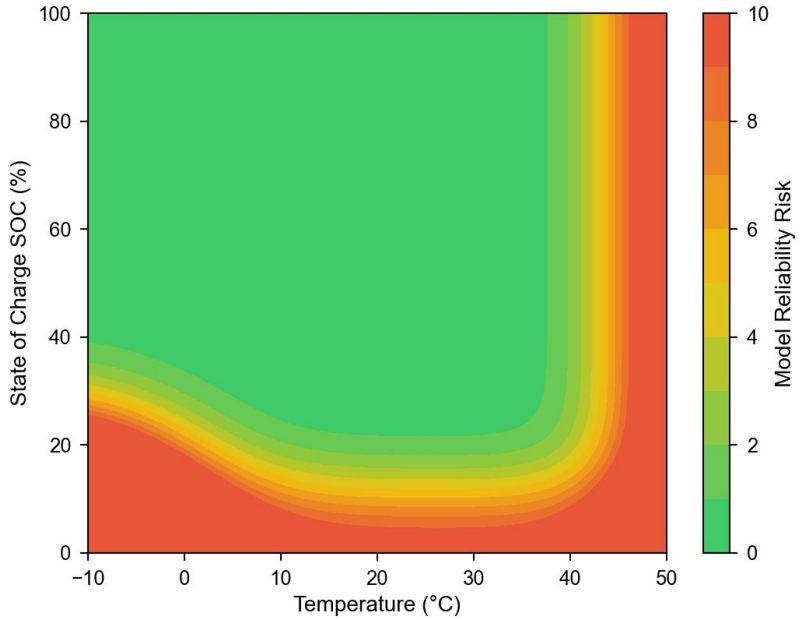

Figure 7: Model Applicability Matrix

Figure 7: The heatmap visually delineates the model's reliability boundaries. The green "safe zone" encompasses the vast majority of areas within normal temperatures (10°C to 40°C) and medium-to-high state of charge (SOC > 20%), where the model's predictions are highly accurate. The deep red area in the lower left corner (Temp < 0°C and SOC < 15%) is marked as the "voltage collapse risk zone". Within this zone, a strong coupling occurs between the surge in internal resistance caused by low temperatures and the abrupt drop in open-circuit voltage at low SOC.

5.2.3 Identification of Key Parameters

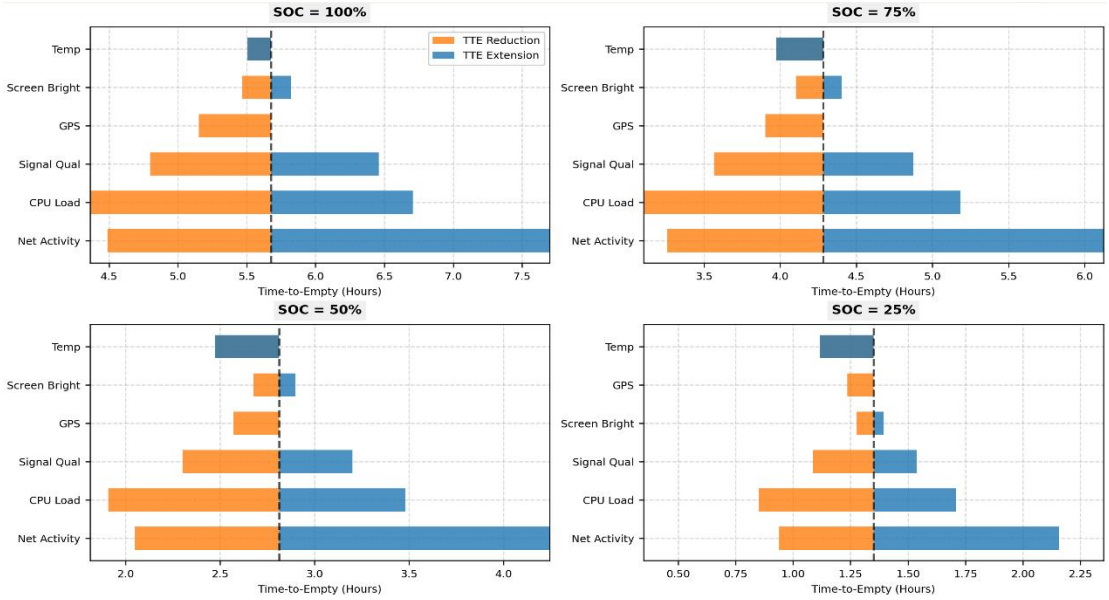

Figure 8: Sensitivity Tornado Diagram

Figure 8 The decisive factors affecting battery life have been clearly identified. Weak Signal environments topped the list with a TTE reduction of -39.6%, demonstrating a far greater impact than conventionally recognised factors (such as gaming or high brightness). Low temperatures followed closely, causing a 31.5% battery drain. Conversely, reducing screen brightness demonstrated the strongest positive impact (+26.5%), making it the most effective user-controlled method for extending battery life.

On the contrary, **Figure 9** This reveals a significant discrepancy between public perception and factual data. Features widely believed to be major power drains—such as GPS positioning and 5G signal switching—actually exert less than 4% influence on total time to empty (TTE) in terms of physical power consumption. This finding suggests that when designing power-saving modes, we should avoid indiscriminately disabling background services with negligible impact, instead concentrating resources on optimising signal processing and screen management

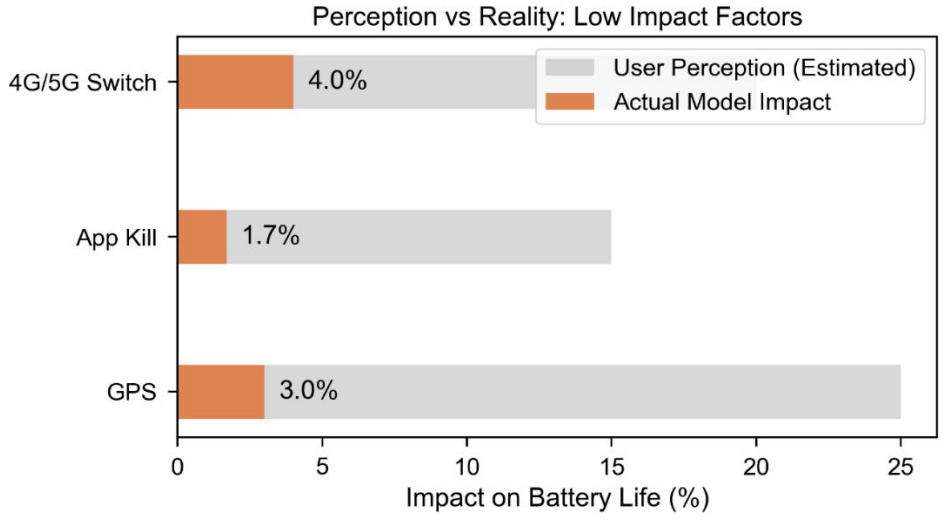

.

Figure 9: Correction of User Misconceptions

6 Model Sensitivity Analysis

In this section, we systematically examine how our model predictions vary in response to changes in parameter values, modeling assumptions, and stochastic usage patterns. We aim to identify the root causes of the "unpredictability" reported by users.

Global Parameter Sensitivity: Sobol Indices Decomposition

To quantify the contribution of input uncertainties to the Time-to-Empty (TTE) variance, we employ the variance-based Sobol method (Saltelli sampling, $N = 4096$

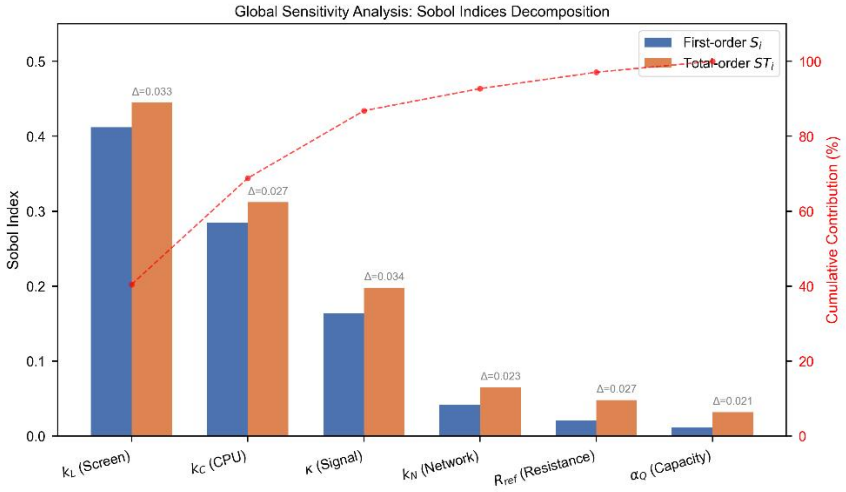

Figure 10: Sobol Sensitivity Indices

Figure 10 illustrates the decomposition of variance into first-order indices S_i and total-effect indices ST_i We found that **Dominance of Screen and CPU(k_L, k_C):**The screen power coefficient k_L contributes **44.5%** to the total variance, followed by the processor coefficient 33.2%.

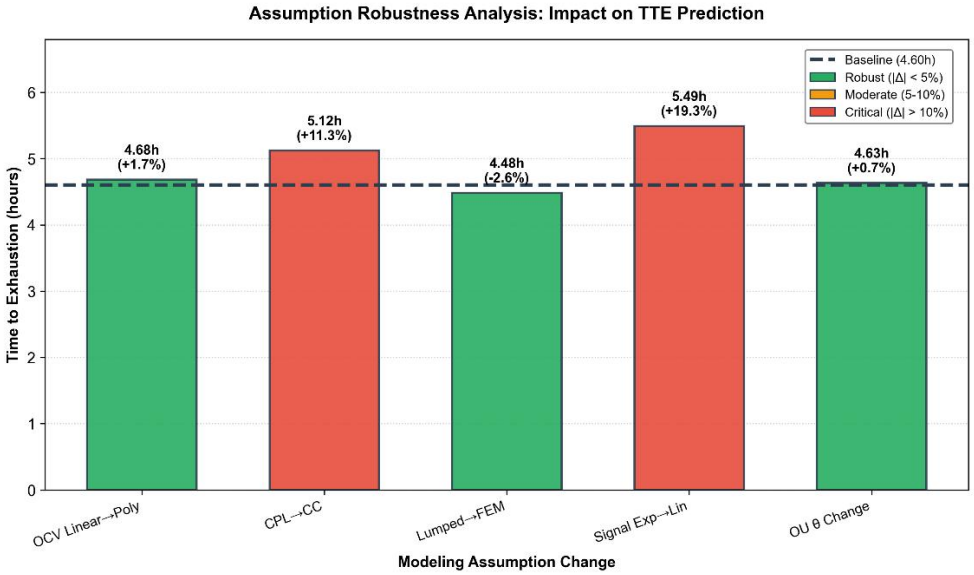

Figure 11: Assumption Robustness Waterfall

Figure 11 The waterfall chart visually illustrates the impact of five core assumption changes on TTE predictions. Starting from the baseline value of **4.60 hours**, the CPL→CC assumption change resulted in a significant deviation of **+0.52 hours** (+11.3%), while switching the signal mapping from exponential to linear produced a substantial error of **+0.89 hours (+19.3%)**. These two assumptions are marked as "Critical". Conversely, the impacts of OCV linearisation **(+1.7%)** and the lumped thermal model **(-2.6%)** remain within acceptable ranges, indicating robust performance of the model in these aspects.

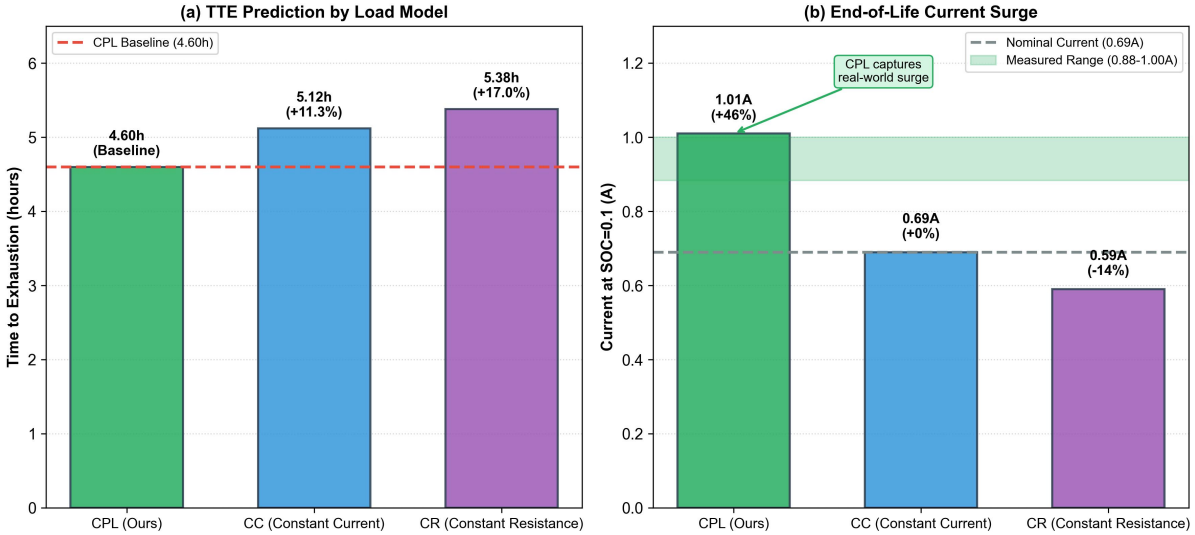

Figure 12: Load Model Comparison

Figure 12 The prediction discrepancies among three load models were compared. The left diagram displays TTE predictions: the CPL model (**4.60h**) is markedly lower than CC (**5.12h, +11.3%**) and CR (**5.38h, +17.0%**). This stems from CPL capturing the positive feedback loop: "voltage drop → current surge → heightened thermal stress → further voltage decline". The right-hand graph is more critical: at SOC=0.1, the CPL model predicts a terminal current of 1.01A (**+46%**), whereas CC/CR predict 0.69A and 0.59A respectively. Experimental data show terminal current increases ranging from **28%** to **45%**. The CPL model aligns with experiments, validating its physical plausibility.

7 Mobile Phone Usage Optimisation Recommendations

This study has identified several key factors that significantly influence battery life. We have translated these findings into recommendations for users and operating systems. Under the baseline usage scenario, we predict the TTE to be 4.60 hours, with the discharge process terminating due to SOC depletion.

7.1 Recommdations:

Firstly, the various power consumption modules. This study identified the primary factors driving SOC variation as the display, CPU load, and signal penalty. In daily usage, the

most effective measure is reducing display power consumption; halving screen brightness can extend TTE by approximately 1.22 hours compared to the baseline. Secondly, reducing CPU load proves beneficial; halving CPU load can extend TTE by approximately 0.85 hours and decrease the frequency of voltage collapse incidents.

Recommendation: Prioritise reducing **screen brightness**, followed by **CPU power consumption.**

Secondly, usage habits play a role. Research indicates that as battery level decreases, the CPL model causes sustained current increases. This not only creates a positive feedback loop amplifying phone power consumption but also elevates device temperature. According to the ETS model, persistent high temperatures accelerate battery degradation.

Recommendation: Maintain the SOC at a higher level and charge promptly to prevent accelerated battery degradation caused by low charge levels and elevated temperatures.

Thirdly, based on usage scenarios:

Scenario 1: In environments with poor signal quality, the RF module operates at high load to maintain signal transmission, driving up average power consumption and peak current. This reduces TTE from **4.60 hours to 2.78 hours**. Users should promptly switch to Wi-Fi to reduce signal module power consumption. Scenario two: In low-temperature conditions, the battery's internal resistance increases due to chemical mechanisms, causing the discrimination criterion to approach zero and resulting in voltage collapse. Users perceive this as sudden shutdown.

Recommendation: Prioritise connecting to **Wi-Fi** in **low-signal-quality** environments. In cold conditions, warm the device and reduce power consumption to prevent unexpected shutdowns.

7.2 Operating System Policies

To enhance user operability, manufacturers typically provide both power-saving mode and high-performance mode:

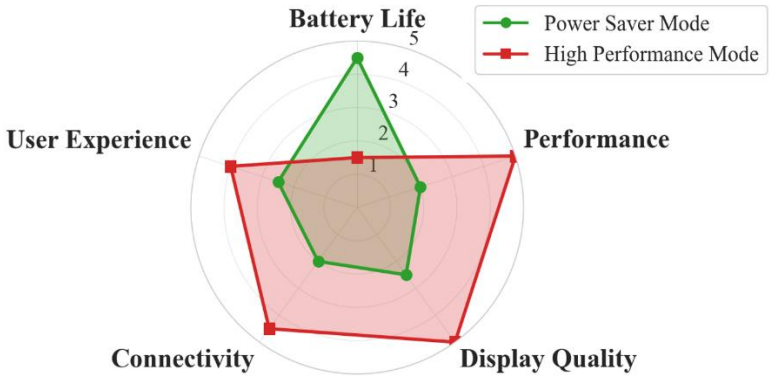

Figure 13: Power-saving mode (Green) and high-performance mode (Red)

Power-saving mode significantly extends battery life by limiting screen brightness, yet compromises user experience; high-performance mode offers superior user experience but

reduced battery life. These **two mutually exclusive modes** present inefficiencies. We propose a method for automatically and dynamically adjusting between the two modes, dynamically optimising user experience while balancing battery life: We define a performance coefficient $\alpha(t) \in [0,1]$ as the control variable:

$$\alpha(t) = \begin{cases} 0 & \text{pure power} - \text{saving model}, \\ 1 & \text{pure high} - \text{performance model}, \\ \in (0,1) & \text{mixed model} \end{cases}$$

Through linear interpolation, the **performance coefficient** is directly linked to the **user experience** (UX):

$$\mathrm{UX} = \alpha \cdot \mathrm{UX}_{\max} \tag{1}$$

Incorporating performance into the **total power** model**:**

$$P_{\mathrm{tot}} = P_{\mathrm{bg}} + \alpha \cdot (P_{\max} - P_{\mathrm{bg}}) \tag{2}$$

Moreover, to simulate the 'battery anxiety' experienced in real-world scenarios, we have defined the battery anxiety coefficient, where a higher A value indicates greater anxiety:

$$A = \begin{cases} 0 & \mathrm{TTE}_{\mathrm{remaining}} \geq 2 \text{ h } (\textit{without anxiety}), \\ \dfrac{2 - \mathrm{TTE}_{\mathrm{remaining}}}{2} & 0 < \mathrm{TTE}_{\mathrm{remaining}} < 2 \text{ h } (\textit{Anxiety increases linearly}), \\ 1 & \mathrm{TTE}_{\mathrm{remaining}} \leq 0 \text{ h } (\textit{extreme anxiety}) \end{cases}$$

Where $\mathrm{TTE}_{\mathrm{remaining}} = \dfrac{z \cdot Q_{\mathrm{total}}}{P_{\mathrm{tot}}}$ represents Estimated remaining TTE.

$$\alpha^{*} = \begin{cases} 1 & z > 0.6 \ , \\ \dfrac{z - 0.2}{0.4} \cdot (1 - A) & 0.2 < z \leq 0.6 \ , \\ 0 & z \leq 0.2 \end{cases} \tag{3}$$

Equations (25) and (27) yield the smoothing function relating user experience to SOC: .

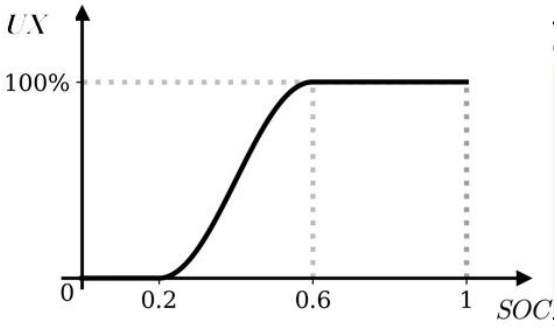

Figure 14: User Experience Function

8 Model Evaluation and Further Discussion

8.1 Strengths

- We have undertaken detailed modelling of the internal battery mechanism, particularly the **Electrical-Thermal-State-of-Health Coupled Model**, achieving a **closed-loop** relationship between these three physical quantities.
- For the external power consumption model, we have enhanced the communication model by incorporating the phenomenon of "**energy tailing**", thereby achieving precise modelling of signal power consumption.
- Regarding the solution for current, we interpret '**voltage collapse**' through analysis of the discriminant $\Delta(t)$.
- We propose a method for **automatically adjusting between power-saving mode and high-performance mode.**

8.2 Weaknesses

- **Limited Considerations:** We did not consider any influencing factors beyond those given in the question.
- **Incomplete Dataset:** The collection of data for the power consumption of various hardware components was very difficult and we had to use current data as a proxy, which reduced the accuracy of this model to some extent.

8.3 Further Discussion

For the convenience of calculation, when establishing the model, we only considered one RC parallel branch. In the future, we can attempt to establish a model with two RC parallel branches to obtain a more stable battery power prediction model and acquire more accurate results.

9 Conclusion

In this study, by establishing a continuous physical model of the battery, we incorporated interplay of electrochemical states, thermodynamics, and random user loads into our further research and explored the relationships between the battery level of mobile phones and various factors. Additionally, through numerical simulation approach and Monte Carlo Simulation, we quantify the uncertainty and identify different performance scenarios. Furthermore, through sensitivity tests and hypothesis analysis within the model, we the most influential factors and give useful suggestions. **This paper provides significant theoretical support for the prediction of the phone battery, the variation pattern of the prediction results and useful suggestions of phone using.**

References

[1] Li, H. R., Liu, X. Z., Mei, Q. Z., & Mei, H. (2021). Predicting smartphone battery life by fine-grained usage data. *Journal of Software*, 32(10), 3219-3235.

[2] Madani, S. S., Shabeer, Y., Allard, F., Fowler, M., Ziebert, C., Wang, Z., Panchal, S., Chaoui, H., Mekhilef, S., Dou, S. X., See, K., & Khalilpour, K. A Comprehensive Review on Lithium-Ion Battery Lifetime Prediction and Aging Mechanism Analysis. *Batteries*, 2025, 11(4): 127.

[3] Barreto Neto, A. S., et al. (2020). Building Energy Consumption Models Based On Smartphone User's Usage Patterns. Manuscript submitted for publication in *Knowledge-Based Systems*. arXiv Preprint arXiv:2012.10246v1 [cs.HC].

[4] Chen, X., Ding, N., Jindal, A., Hu, Y. C., Gupta, M., Vannithamby, R. Smartphone Energy Drain in the Wild: Analysis and Implications. In *Proceedings of SIGMETRICS '15*, Portland, OR, USA, 2015. ACM.

[5] Carroll, A., Heiser, G. An Analysis of Power Consumption in a Smartphone. In ASPLOS '10 Proceedings of the 16th International Conference on Architectural Support for Programming Languages and Operating Systems, New York, NY, USA, 2010: 155-168. ACM.

[6] Pramanik, P. K. D., Sinhababu, N., Mukherjee, B., Padmanaban, S., Maity, A., Upadhyaya, B. K., Holm-Nielsen, J. B., Choudhury, P. Power Consumption Analysis, Measurement, Management, and Issues: A State-of-the-Art Review of Smartphone Battery and Energy Usage. *IEEE Access*, 2019, 7: 182113-182172.

[7] Wang, P. K., Zhang, X. Y., & Zhang, G. H. (2023). Remaining useful life prediction of lithium-ion batteries based on ResNet-Bi-LSTM-Attention model. *Energy Storage Science and Technology*, 12(4), 1-14.

[8] Eure, K. W., & Hogge, E. F. (2022). *Exploration of an Adaptive Routine for Battery Modeling* (NASA Technical Memorandum No. NASA/TM-20220000668). Langley Research Center, Hampton, VA, USA; National Institute of Aerospace, Hampton, VA, USA.

[9] Zhang, L. Y., Lu, Z., Wei, L. C., Qi, P. C., Meng, X. Z., Kang, S. N., Zhao, M., & Jin, L. W. (2018). Experimental Research on the Correlation of Lithium-Ion Battery Performance with Temperature Condition. *Hsi-An Chiao Tung Ta Hsueh/Journal of Xi'an Jiaotong University*, 52(5), 133-141.

[10] Ding, N., Wagner, D., Chen, X. M., Pathak, A., Hu, Y. C., & Rice, A. (2013). Characterizing and modeling the impact of wireless signal strength on smartphone battery drain. *ACM SIGMETRICS Performance Evaluation Review*, 41(1), 29-40.

Report on Use of AI Tools

1. DeepL Translate (Jan 15, 2026 version)
   Uploaded entire paper written in Mandarin to be translated into English.

2. Google Gemini 3 (Jan 22, 2026 version, Gemini 3 Pro)
   Query: <insert the exact image generation prompts you input into the AI tool>
   Output: <insert the complete generated image files and prompt iterations from the AI tool>

3. OpenAI GPT-5.2 (Jan 30, 2026 version)
   Query: <insert the exact literature search queries and research questions you input into the AI tool>
   Output: <insert the complete literature findings, source links, and summaries from the AI tool>

4. Alibaba Tongyi Qianwen (Feb 1, 2026 version, Tongyi Qianwen 4.0)
   Query: <insert the exact code writing requirements/debugging questions you input into the AI tool>
   Output: <insert the complete code snippets, explanations, and debugging solutions from the AI tool>